On the advantages of using the first-order generalised-alpha scheme for structural dynamic problems

C. Kadapa*, W. G. Dettmer, D. Perić

Zienkiewicz Centre for Computational Engineering, College of Engineering, Swansea University, Fabian Way, Swansea, SA1 8EN, Wales, UK.

Abstract

The advantages of using the generalised-alpha scheme for first-order systems for computing the numerical solutions of second-order equations encountered in structural dynamics are presented. The governing equations are rewritten so that the second-order equations can be solved directly without having to convert them into state-space. The stability, accuracy, dissipation and dispersion characteristics of the scheme are discussed. It is proved through spectral analysis that the proposed scheme has improved dissipation properties when compared with the standard generalised-alpha scheme for second-order equations. It is also proved that the proposed scheme does not suffer from overshoot. Towards demonstrating the application to practical problems, proposed scheme is applied to the benchmark example of three degrees of freedom stiff-flexible spring-mass system, two-dimensional Howe truss model, and elastic pendulum problem discretised with non-linear truss finite elements.

Keywords: Structural dynamics; Time integration; Generalised-alpha scheme; Numerical dissipation; Overshoot

1. Introduction

Obtaining stable and accurate solutions of second-order dynamical systems encountered in science and engineering has been one of the important areas of research on numerical schemes for initial value problems (IVPs). In literature, there are several time integration schemes for solving structural dynamic problems. Several classifications exist for such schemes: *implicit* or *explicit* and *single-step* or *multi-step* being the most prominent ones. The detailed discussion of such schemes is beyond the scope of this paper and any standard book on numerical schemes for initial value problems, e.g. [1–7], may be consulted for this purpose.

Implicit schemes generally possess better stability characteristics than explicit schemes. An implicit scheme allows using large steps for obtaining numerical solutions, hence, such schemes require less time and effort. However, it is now an established fact that use of large time steps, in implicit schemes, results in undesirable numerical dissipation in the low-frequency range. On the other hand, for structural dynamics problems discretised with finite

*Corresponding author
Email address: c.kadapa@swansea.ac.uk (C. Kadapa)

elements, it is advantageous to be able to control the amount of numerical damping so that adverse effects of spurious higher-frequency modes on the numerical solution can be avoided. Therefore, a time integration scheme with controllable numerical damping for high-frequency modes and at the same time with less numerical dissipation in the low-frequency range is desirable. Following Hilber and Hughes [7, 8], a competitive numerical scheme for structural dynamic problems should possess the following important characteristics:

1. Unconditional stability when applied to a linear problem.
2. No more than one set of implicit equations should have to be solved at each time step.
3. Second-order accuracy.
4. Controllable algorithmic dissipation in the higher modes.
5. Self-starting.
6. The scheme should not suffer from *overshoot* behaviour.

A considerable amount of research has gone into developing implicit schemes which possess the above-listed attributes. Newmark-β scheme [9], Wilson-θ scheme [10], HHT-α scheme [11], Collocation scheme [8], WBZ-α scheme [12], HP-θ_1 scheme [13], CH-α scheme [14] and G-α scheme [15] are few such schemes which satisfy some or all of the above listed criteria. Though all these schemes are unconditionally stable, implicit, single-step and second-order in nature, their differences are in the amount of numerical dissipation and whether or not they suffer from overshoot. HHT-α, CH-α and WBZ-α schemes have been proven to suffer from overshooting, see [15] and references therein. Erlicher et al. [16] have proven the overshoot behaviour of CH-α scheme in the context of non-linear dynamic problems. KaiPing [15] has improved upon CH-α scheme and devised a new family of generalised-α schemes without overshoot. Though NOHHT-α and NOWBZ-α schemes, proposed by [15], are without overshoot and have better dissipation properties when compared with their counterparts with overshoot, the amount of numerical dissipation of NOCH-α remained exactly same as that of the CH-α scheme. On the similar lines, Kuhl and Crisfield [17] developed energy conserving generalised energy-momentum methods based on CH-α scheme.

It is important to note that all the schemes listed above are single-step schemes for second-order IVPs. To the knowledge of the authors, there are only a few direct multi-step schemes for second-order IVPs. Two-step composite scheme by Bathe and Baig [18] and the three-step scheme by Wen et al. [19] are two such multi-step schemes for structural dynamic problems. We refer to a recent article by Zhang et al. [20] for a comprehensive numerical analysis of such composite schemes. Though these multi-step schemes do not contain any adjustable parameter, their main disadvantage is that for the same time step size, they are computationally expensive when compared with single-step schemes. For example, for a linear problem, and for a given time step, the computational cost of Bathe's two-step scheme is twice that of a single-step scheme; and for the three-step scheme by Wen et al. [19] the computational cost is three times that of a single-step scheme. In addition, the task of book-keeping and storing variables for intermediate

steps in multi-step schemes adds to unnecessary computational overheads. Furthermore, the cost and complexity of the algorithm of multi-step schemes increase many folds for non-linear problems.

In this paper, we propose to use the generalised-α scheme for the first-order dynamic systems, proposed by Jansen et al. [21] and referred as JWH-α from this point onwards, for obtaining the numerical solutions of structural dynamic problems. Recently, this scheme has been applied to nearly incompressible elasticity by Rossi et al. [22] and viscoelasticity by Zeng et al. [23]. This work is motivated by the need for a consistent time integration scheme for fluid-structure interaction (FSI) problems. CH-α and JWH-α schemes have been extensively used as time integration schemes for fluid and solid sub-problems, respectively, in numerical schemes for coupled fluid-structure interaction, see [24–30]. Investigation of time integration schemes for fluids [24] showed the excellent performance of the JWH-α scheme. Dettmer and Perić [31] used CH-α and JWH-α schemes, respectively, for fluid and solid sub-solvers to obtain second order accurate unconditionally stable weakly coupled solution scheme for FSI with small to moderate added mass effects. All of these motivate the development of the unified framework proposed in present work in which a single time integration scheme is used for both fluid and solid sub-problems.

The outline of the paper is as follows. The governing equations and proposed scheme are presented in Section 2. Stability and accuracy analysis are carried out in Section 3. Dissipation and dispersion characteristics of the scheme are studied in Section 4. In Section 5, it is proved that the proposed scheme does not suffer from overshoot behaviour. Finally, the algorithm is applied to three multi-degree of freedom (MDOF) examples in Section 6 and the performance of the proposed scheme is compared against CH-α and Bathe's schemes. Conclusions are drawn in Section 7.

2. Governing equations and the proposed time integration scheme

The governing equation for the general linear structural dynamic problem can be written in matrix-vector form as,

$$\mathbf{M}\,\ddot{\mathbf{d}} + \mathbf{C}\,\dot{\mathbf{d}} + \mathbf{K}\,\mathbf{d} = \mathbf{F} \tag{1}$$

$$\mathbf{d}(t=0) = \mathbf{d}_0 \tag{2}$$

$$\dot{\mathbf{d}}(t=0) = \dot{\mathbf{d}}_0 \tag{3}$$

where, $\mathbf{M}$, $\mathbf{C}$ and $\mathbf{K}$ are the mass, damping and stiffness matrices, respectively; $\mathbf{d}$ is the vector of displacements (including rotational degree of freedom) and $\dot{\mathbf{d}} = \mathrm{d}\mathbf{d}/\mathrm{d}t$, $\ddot{\mathbf{d}} = \mathrm{d}^2\mathbf{d}/\mathrm{d}t^2$ are the velocity and acceleration vectors; $\mathbf{F}$ is the vector of external nodal forces; $\mathbf{d}_0$ and $\dot{\mathbf{d}}_0$ are the initial displacement and velocity, respectively. In order for the formulation to be consistent and balance total energy, the initial acceleration should be computed as,

$$\ddot{\mathbf{d}}_0 = \mathbf{M}^{-1}\left[\mathbf{F}(t=0) - \mathbf{C}\,\dot{\mathbf{d}}_0 - \mathbf{K}\,\mathbf{d}_0\right] \tag{4}$$

In order to apply the JWH-α scheme, the second-order equation Eq. (1) is first converted into a system of first-order equations. By introducing an auxiliary variable $\mathbf{v} = \dot{\mathbf{d}}$, the equivalent first-order system can be written in the matrix form as,

$$\begin{bmatrix} \mathbf{M} & \mathbf{0} \\ \mathbf{0} & \mathbf{M} \end{bmatrix} \begin{Bmatrix} \dot{\mathbf{d}} \\ \dot{\mathbf{v}} \end{Bmatrix} + \begin{bmatrix} \mathbf{0} & -\mathbf{M} \\ \mathbf{K} & \mathbf{C} \end{bmatrix} \begin{Bmatrix} \mathbf{d} \\ \mathbf{v} \end{Bmatrix} = \begin{Bmatrix} \mathbf{0} \\ \mathbf{F} \end{Bmatrix} \tag{5}$$

By applying the JWH-α scheme to Eq. (5), the following first-order system is obtained.

$$\begin{bmatrix} \mathbf{M} & \mathbf{0} \\ \mathbf{0} & \mathbf{M} \end{bmatrix} \begin{Bmatrix} \dot{\mathbf{d}}_{n+\alpha_m} \\ \dot{\mathbf{v}}_{n+\alpha_m} \end{Bmatrix} + \begin{bmatrix} \mathbf{0} & -\mathbf{M} \\ \mathbf{K} & \mathbf{C} \end{bmatrix} \begin{Bmatrix} \mathbf{d}_{n+\alpha_f} \\ \mathbf{v}_{n+\alpha_f} \end{Bmatrix} = \begin{Bmatrix} \mathbf{0} \\ \mathbf{F}_{n+\alpha_f} \end{Bmatrix} \tag{6}$$

with,

$$\dot{\mathbf{d}}_{n+\alpha_m} = \alpha_m \, \dot{\mathbf{d}}_{n+1} + (1-\alpha_m) \, \dot{\mathbf{d}}_n \tag{7}$$

$$\dot{\mathbf{v}}_{n+\alpha_m} = \alpha_m \, \dot{\mathbf{v}}_{n+1} + (1-\alpha_m) \, \dot{\mathbf{v}}_n \tag{8}$$

$$\mathbf{d}_{n+\alpha_f} = \alpha_f \, \mathbf{d}_{n+1} + (1-\alpha_f) \, \mathbf{d}_n \tag{9}$$

$$\mathbf{v}_{n+\alpha_f} = \alpha_f \, \mathbf{v}_{n+1} + (1-\alpha_f) \, \mathbf{v}_n \tag{10}$$

$$\mathbf{F}_{n+\alpha_f} = \alpha_f \, \mathbf{F}_{n+1} + (1-\alpha_f) \, \mathbf{F}_n \tag{11}$$

$$\mathbf{d}_{n+1} = \mathbf{d}_n + \Delta t \left[\gamma \, \dot{\mathbf{d}}_{n+1} + (1-\gamma) \, \dot{\mathbf{d}}_n \right] \tag{12}$$

$$\mathbf{v}_{n+1} = \mathbf{v}_n + \Delta t \left[\gamma \, \dot{\mathbf{v}}_{n+1} + (1-\gamma) \, \dot{\mathbf{v}}_n \right] \tag{13}$$

For convenience, Eqs. (12) and (13) are rewritten as,

$$\dot{\mathbf{d}}_{n+1} = \frac{1}{\gamma \Delta t} \left[\mathbf{d}_{n+1} - \mathbf{d}_n \right] + \frac{\gamma - 1}{\gamma} \, \dot{\mathbf{d}}_n \tag{14}$$

$$\dot{\mathbf{v}}_{n+1} = \frac{1}{\gamma \Delta t} \left[\mathbf{v}_{n+1} - \mathbf{v}_n \right] + \frac{\gamma - 1}{\gamma} \, \dot{\mathbf{v}}_n \tag{15}$$

Now, using the Eqs. (7)-(13), the first-order matrix system Eq. (6) can be solved for $\{\mathbf{d}_{n+1} \ \mathbf{v}_{n+1}\}^T$. However, this is not a wise choice as this would require solving a matrix system which is twice as large as the original one. Even though the resulting overhead might be insignificant for small problems, the cost would increase substantially for large problems, especially when the matrix system needs to be solved at every iteration of every time step for a non-linear problem. Therefore, in the present work, we rewrite the Eq. (6) so that we only need to solve a matrix system that is exactly the same size as that of the original system.

A close observation of Eq. (6) reveals that, its first equation can be simplified to an equation involving only vectors. Accordingly, we get,

$$\dot{\mathbf{d}}_{n+\alpha_m} = \mathbf{v}_{n+\alpha_f} \tag{16}$$

which, using Eqs. (7) and (10) in Eq. (6), can be rearranged as,

$$\mathbf{v}_{n+1} = \frac{\alpha_m}{\alpha_f}\,\dot{\mathbf{d}}_{n+1} + \frac{1-\alpha_m}{\alpha_f}\,\dot{\mathbf{d}}_n + \frac{\alpha_f - 1}{\alpha_f}\,\mathbf{v}_n \tag{17}$$

Now, using Eqs. (14), (15) and (17), $\mathbf{v}_{n+1}$ and $\dot{\mathbf{v}}_{n+1}$ become,

$$\mathbf{v}_{n+1} = \frac{\alpha_m}{\alpha_f\gamma\Delta t}\,(\mathbf{d}_{n+1} - \mathbf{d}_n) + \frac{(\gamma-\alpha_m)}{\gamma\alpha_f}\,\dot{\mathbf{d}}_n + \frac{(\alpha_f-1)}{\alpha_f}\mathbf{v}_n \tag{18}$$

$$\dot{\mathbf{v}}_{n+1} = \frac{\alpha_m}{\alpha_f\gamma^2\Delta t^2}\,(\mathbf{d}_{n+1} - \mathbf{d}_n) - \frac{1}{\alpha_f\gamma\Delta t}\,\mathbf{v}_n + \frac{\gamma-1}{\gamma}\,\dot{\mathbf{v}}_n + \frac{(\gamma-\alpha_m)}{\alpha_f\gamma^2\Delta t}\,\dot{\mathbf{d}}_n \tag{19}$$

Finally, using Eqs. (8), (9), (10), (18) and (19), the second equation of Eq. (6),

$$\mathbf{M}\dot{\mathbf{v}}_{n+\alpha_m} + \mathbf{C}\,\mathbf{v}_{n+\alpha_f} + \mathbf{K}\,\mathbf{d}_{n+\alpha_f} = \mathbf{F}_{n+\alpha_f} \tag{20}$$

can be solved for $\mathbf{d}_{n+1}$ from,

$$\hat{\mathbf{K}}\,\mathbf{d}_{n+1} = \hat{\mathbf{F}} \tag{21}$$

where, the effective stiffness matrix, $\hat{\mathbf{K}}$, and the effective force vector, $\hat{\mathbf{F}}$, are given as,

$$\hat{\mathbf{K}} = \frac{\alpha_m^2}{\alpha_f\gamma^2\Delta t^2}\mathbf{M} + \frac{\alpha_m}{\gamma\Delta t}\mathbf{C} + \alpha_f\mathbf{K} \tag{22}$$

$$\begin{aligned}\hat{\mathbf{F}} = {} & \mathbf{F}_{n+\alpha_f} - (1-\alpha_m)\mathbf{M}\dot{\mathbf{v}}_n - (1-\alpha_f)\mathbf{C}\mathbf{v}_n - (1-\alpha_f)\mathbf{K}\mathbf{d}_n \\ & + \alpha_f\mathbf{C}\left[\frac{\alpha_m}{\alpha_f\gamma\Delta t}\,\mathbf{d}_n - \frac{(\gamma-\alpha_m)}{\gamma\alpha_f}\,\dot{\mathbf{d}}_n - \frac{(\alpha_f-1)}{\alpha_f}\mathbf{v}_n\right] \\ & + \alpha_m\mathbf{M}\left[\frac{\alpha_m}{\alpha_f\gamma^2\Delta t^2}\,\mathbf{d}_n + \frac{1}{\alpha_f\gamma\Delta t}\,\mathbf{v}_n - \frac{\gamma-1}{\gamma}\,\dot{\mathbf{v}}_n - \frac{(\gamma-\alpha_m)}{\alpha_f\gamma^2\Delta t}\,\dot{\mathbf{d}}_n\right]\end{aligned} \tag{23}$$

Once $\mathbf{d}_{n+1}$ is obtained, $\dot{\mathbf{d}}_{n+1}$, $\mathbf{v}_{n+1}$and $\dot{\mathbf{v}}_{n+1}$ can be computed from Eqs. (14), (18) and (19), respectively. In this way, we will only solve a matrix system whose size is same as that of the original system (1). The only additional cost involved is storage memory for a single new variable $\dot{\mathbf{d}}_n$, and scalar-vector computations in evaluating $\dot{\mathbf{d}}_{n+1}$ from Eq. (14).

2.1. The algorithm for non-linear problems

Assuming that mass and damping are linear, the governing equations for a non-linear structural dynamic problem can be written as,

$$\mathbf{M}\dot{\mathbf{v}}_{n+\alpha_m} + \mathbf{C}\,\mathbf{v}_{n+\alpha_f} + \mathbf{G}_{n+\alpha_f} = \mathbf{F}_{n+\alpha_f} \tag{24}$$

where, $\mathbf{G}_{n+\alpha_f}$ is the vector of internal forces, and it is decomposed as,

$$\mathbf{G}_{n+\alpha_f} = \alpha_f\,\mathbf{G}_{n+1} + (1-\alpha_f)\,\mathbf{G}_n = \alpha_f\,\mathbf{G}(\mathbf{d}_{n+1}) + (1-\alpha_f)\,\mathbf{G}(\mathbf{d}_n) \tag{25}$$

As the system of equations (24) is non-linear, Newton-Raphson scheme is used in the present work. The vector of residuals, at iteration $(k+1)$ of time step t_{n+1}, for Eq. (24) can be written as,

$$\mathbf{R}(\mathbf{d}_{n+1}^{(k+1)}) = \mathbf{F}_{n+\alpha_f}^{(k+1)} - \mathbf{M}\dot{\mathbf{v}}_{n+\alpha_m}^{(k+1)} - \mathbf{C}\,\mathbf{v}_{n+\alpha_f}^{(k+1)} - \mathbf{G}_{n+\alpha_f}^{(k+1)} \tag{26}$$

Applying Newton-Raphson scheme to solve the non-linear set of equations (26), it follows,

$$\hat{\mathbf{K}}(\mathbf{d}_{n+1}^{(k)})\,\Delta\mathbf{d} = -\mathbf{R}(\mathbf{d}_{n+1}^{(k)}) \tag{27}$$

where, $\hat{\mathbf{K}}(\mathbf{d}_{n+1}^{(k)})$ and $\mathbf{R}(\mathbf{d}_{n+1}^{(k)})$ are the effective stiffness matrix and residual vector at iteration $(k+1)$, and $\Delta\mathbf{d} = \mathbf{d}_{n+1}^{(k+1)} - \mathbf{d}_{n+1}^{(k)}$ is the incremental displacement vector. The effective stiffness matrix is computed as,

$$\hat{\mathbf{K}} = \frac{\alpha_m^2}{\alpha_f\gamma^2\Delta t^2}\mathbf{M} + \frac{\alpha_m}{\gamma\Delta t}\mathbf{C} + \alpha_f\mathbf{K}^t(\mathbf{d}_{n+1}^k) \tag{28}$$

Here, $\mathbf{K}^t(\mathbf{d}_{n+1}^{(k)})$ is the tangent stiffness and it consists of geometric and material parts which are associated with the choice of finite element discretisation, see [32, 33]. The pseudo code for the application of the present scheme to non-linear problems is given in Algorithm 1.

3. Stability and accuracy analysis

For the purpose of stability and accuracy analysis, we consider the standard single degree of freedom (SDOF) spring-mass-damper system. The governing equation for the standard spring-mass-damper system, without any external force acting on it, is given by,

$$\ddot{d} + 2\,\xi\,\omega\,\dot{d} + \omega^2\,d = 0 \tag{29}$$

Algorithm 1 Algorithm for non-linear problems

Set: ρ_∞, t_0, t_f, Δt and tolerance ϵ
Compute: α_m, α_f and γ
Compute: $\dot{\mathbf{v}}_0 (= \ddot{\mathbf{d}}_0)$ from $\mathbf{d}_0$ and $\dot{\mathbf{d}}_0$.
Set: $\mathbf{v}_0 = \dot{\mathbf{d}}_0$
for $t = t_0$ to $t = t_f$ **do**
    Predict: $\mathbf{d}_{n+1}^{(1)} = \mathbf{d}_n$
    for k=1 to *max-iter* **do**
        Compute: $\mathbf{v}_{n+1}^{(k)}$ and $\dot{\mathbf{v}}_{n+1}^{(k)}$, respectively, from (18) and (19)
        Compute: $\hat{\mathbf{K}}(\mathbf{d}_{n+1}^{k})$ and $\mathbf{R}(\mathbf{d}_{n+1}^{k})$
        if $|\mathbf{R}(\mathbf{d}_{n+1}^{k})| \leq \epsilon$ **then**
            Converged, exit iteration loop
        end if
        Solve: $\hat{\mathbf{K}}(\mathbf{d}_{n+1}^{(k)})\, \Delta\mathbf{d} = -\mathbf{R}(\mathbf{d}_{n+1}^{(k)})$
        Update: $\mathbf{d}_{n+1}^{(k+1)} = \mathbf{d}_{n+1}^{(k)} + \Delta\mathbf{d}$
    end for
    Compute: $\dot{\mathbf{d}}_{n+1}$ from (14)
    $(\mathbf{d}_n, \dot{\mathbf{d}}_n, \mathbf{v}_n, \dot{\mathbf{v}}_n) \leftarrow (\mathbf{d}_{n+1}, \dot{\mathbf{d}}_{n+1}, \mathbf{v}_{n+1}, \dot{\mathbf{v}}_{n+1})$
end for

where, $\omega = \sqrt{k/m}$ is the undamped natural frequency and $\xi = c/(2\sqrt{k\,m})$ is the damping ratio. The natural time period of oscillations is defined as, $T = 2\pi/\omega$. Using equations (7)-(19), the complete solution to equation to Eq. (29) may be written in the form,

$$\mathbf{X}_{n+1} = \mathbf{A}\,\mathbf{X}_n, \quad \forall n \in [0, 1, ..., N-1] \tag{30}$$

where, N is the number of time steps, $\mathbf{X}_i = \{d_i,\ v_i\Delta t,\ \dot{d}_i\Delta t,\ \dot{v}_i\Delta t^2\}^T$ and $\mathbf{A}$ is termed the amplification matrix which is used to assess the performance characteristics of the scheme. It is important to note that the matrix $\mathbf{A}$ for the proposed scheme is of size 4×4 while the amplification matrix for other similar schemes is of size 3×3.

The parameter that aids in the analysis of numerical schemes for stability, accuracy and dissipation properties is *spectral radius*, which is defined as,

$$\rho = \max(|\lambda_1|, |\lambda_2|, |\lambda_3|, |\lambda_4|) \tag{31}$$

where, λ_1, λ_2, λ_3 and λ_4 are the eigenvalues of the amplification matrix $\mathbf{A}$. It can be verified that, as expected, the parameters α_f, α_m and γ need to be chosen as defined in Jansen et al. [21] in order to guarantee second order accuracy, unconditional stability and user controlled high frequency damping. Thus,

$$\alpha_f = \frac{1}{1+\rho_\infty}; \quad \alpha_m = \frac{(3-\rho_\infty)}{2(1+\rho_\infty)}; \quad \gamma = \frac{1}{2} + \alpha_m - \alpha_f \tag{32}$$

where, the parameter ρ_∞ corresponds to the spectral radius at an infinite time step and must be chosen such that $0 \leq \rho_\infty \leq 1$.

4. Numerical dissipation and dispersion analysis

We now present the *numerical dissipation* and *numerical dispersion* properties of the present scheme using the spectral analysis and make comparisons with CH-α and Bathe's schemes. The CH-α scheme is already proven to have better dissipation properties when compared with Newmark-β, HHT-α, WBZ-α and HP-θ_1 schemes, see [14]. Hence, it suffices to use the CH-α scheme as the reference for single-step schemes. In order to compare with the state-of-the-art, we use Bathe's two-step scheme as another reference. For numerical calculations, we take $m = 1$ and $T = 1$ and the value of c is adjusted depending upon the value of damping ratio ξ. The initial conditions are: $d_0 = 1$ and $\dot{d}_0 = 0$.

We compute spectral radius (ρ), time period ($\bar{T} = 2\pi/\bar{\omega}$) and damping ratio ($\bar{\xi}$) of the numerical solution in order to assess the amount of *numerical damping* and *numerical dissipation*. The magnitude of spectral radius indicates the amount of numerical dissipation: the smaller the spectral radius the higher the numerical dissipation. The amount of

numerical dissipation and dispersion are measured by the damping ratio ($\bar{\xi}$) and relative period error ($\frac{\bar{T}-T}{T}$), respectively.

Fig. 1 shows the values of spectral radius, period elongation error and damping ratio error for the case without damping, $\xi = 0.0$, and with damping, $\xi = 0.1$. From these graphs, it can be observed that, for the entire range $\rho_\infty \in [0, 1)$, the proposed scheme has better numerical dissipation and dispersion properties when compared with CH-α scheme. The reduction in dissipation and dispersion errors is more pronounced as $\rho_\infty \to 0$. For the purpose of comparison with Bathe's scheme, two graphs are presented in each figure, one with the same time step as that of the proposed scheme and the second one with twice the time step. This is due to the fact that, for a given time step, Bathe's scheme is computationally twice as expensive as the proposed scheme. From Fig. 1 it is clearly evident that, for the same computational cost, and for $\rho_\infty \geq 0.5$, CH-α and the proposed schemes have lower period elongation and damping ratio errors when compared with Bathe's scheme. These observations have been confirmed by computing numerical solutions of the model problem, as presented in Figures 2 and 3. It is important to mention that the time step used for Bathe's scheme is twice that used for CH-α and present schemes. As shown, solutions obtained with the present scheme converge to the reference solution as $\Delta t \to 0$, illustrating the convergence of the scheme. It can be observed that for $\rho_\infty = 0.5$ and $\Delta t = T/10$, the results obtained with the proposed scheme are slightly better than the ones obtained with Bathe's scheme and match well with those obtained with CH-α scheme; and for $\rho_\infty = 0.0$ and $\Delta t = T/10$, the solutions obtained with the present scheme are poor when compared with Bathe's scheme but still better than the ones obtained with CH-α scheme. Therefore, when the spectral radius (ρ_∞) value is chosen high enough then, for the same computational cost, the present scheme yields better results than Bathe's scheme and when $\rho_\infty \to 0$, the present scheme, although poorer that the Bathe's scheme, yields better results than CH-α scheme.

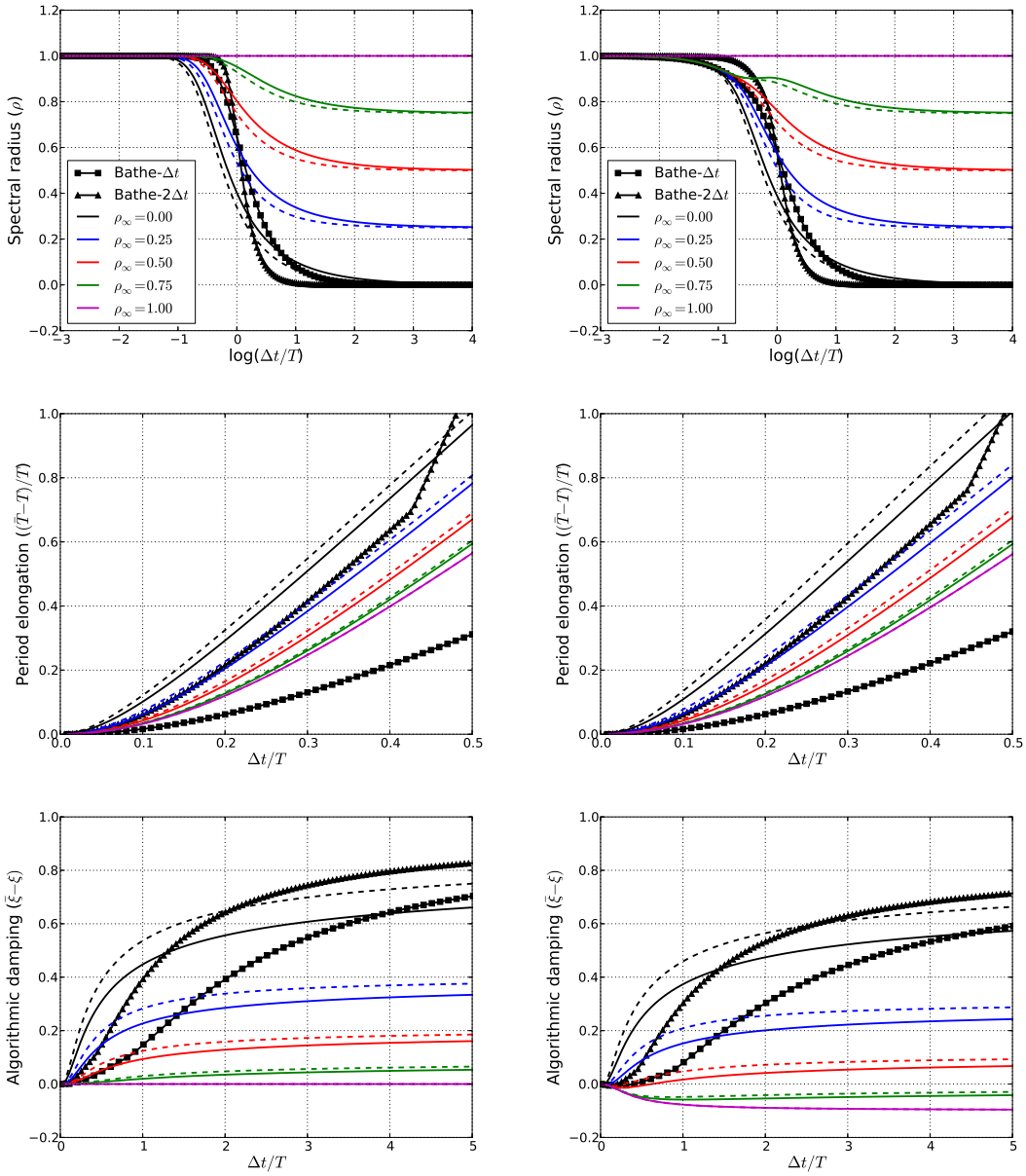

Figure 1: Spectral radius, period elongation error and algorithmic damping versus $\Delta t/T$. Graphs for the case $\xi = 0.0$ are on the left side and the ones for $\xi = 0.1$ are on the right side. Dashed lines are for the CH-α scheme and solid lines for the present scheme.

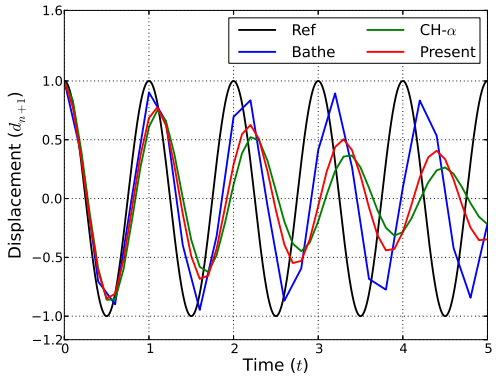

(a) $\rho_\infty = 0.0$, $\Delta t = T/10$

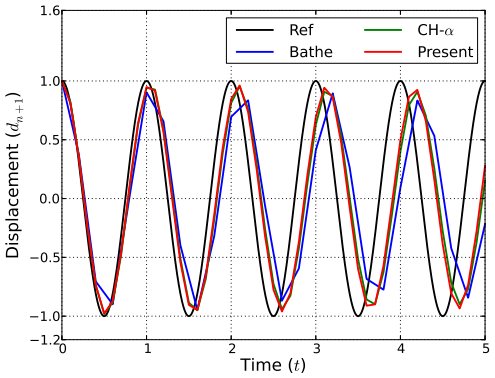

(b) $\rho_\infty = 0.5$, $\Delta t = T/10$

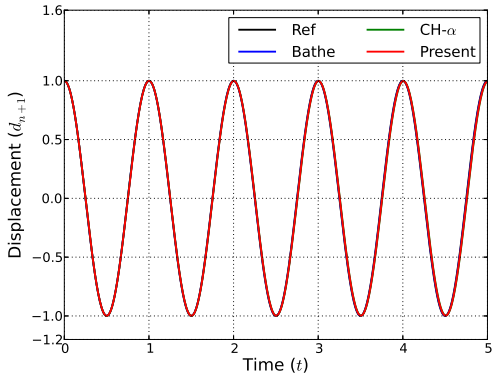

(c) $\rho_\infty = 0.0$, $\Delta t = T/100$

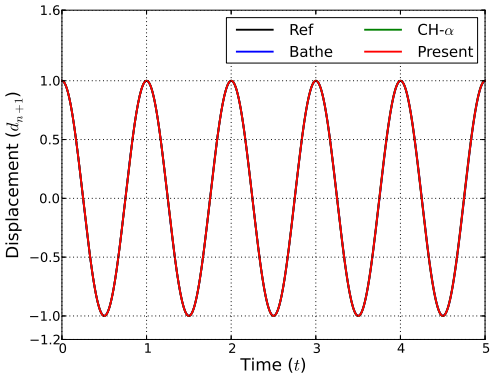

(d) $\rho_\infty = 0.5$, $\Delta t = T/100$

Figure 2: Model problem: displacement obtained for $\xi = 0.0$.

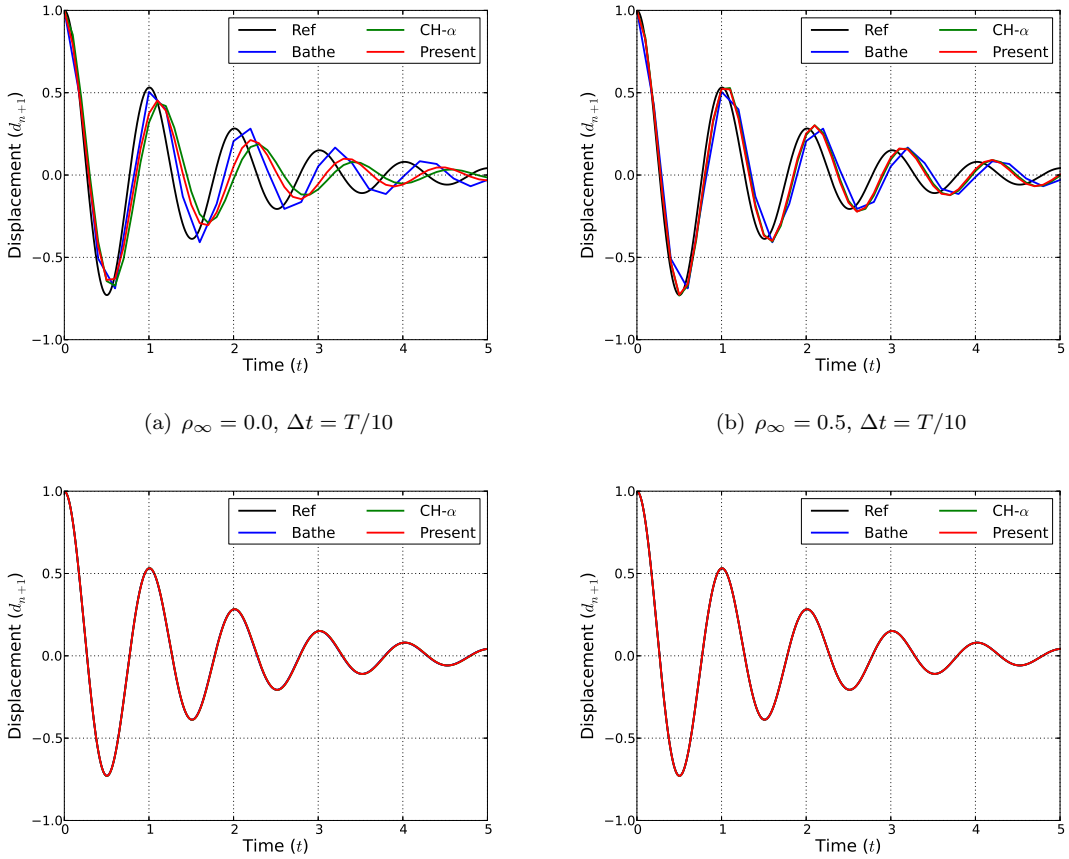

(a) $\rho_\infty = 0.0$, $\Delta t = T/10$

(b) $\rho_\infty = 0.5$, $\Delta t = T/10$

(c) $\rho_\infty = 0.0$, $\Delta t = T/100$

(d) $\rho_\infty = 0.5$, $\Delta t = T/100$

Figure 3: Model problem: displacement obtained for $\xi = 0.1$.

5. Analysis for overshoot

The overshoot behaviour of the scheme is assessed by studying the solution of the model problem at the first time step. Absolute errors in displacement and velocity for the case without physical damping ($\xi = 0$) for $\rho_\infty = 0.0$ and $\rho_\infty = 0.5$ are shown, respectively, in Figs. 4 and 5. The corresponding plots for the case with physical damping ($\xi = 0.1$) are shown in Figs. 6 and 7. These graphs indicate that the present scheme and the Bathe's scheme do not suffer from *overshoot*, while the CH-α scheme shows significant overshoot, particularly for the velocity values.

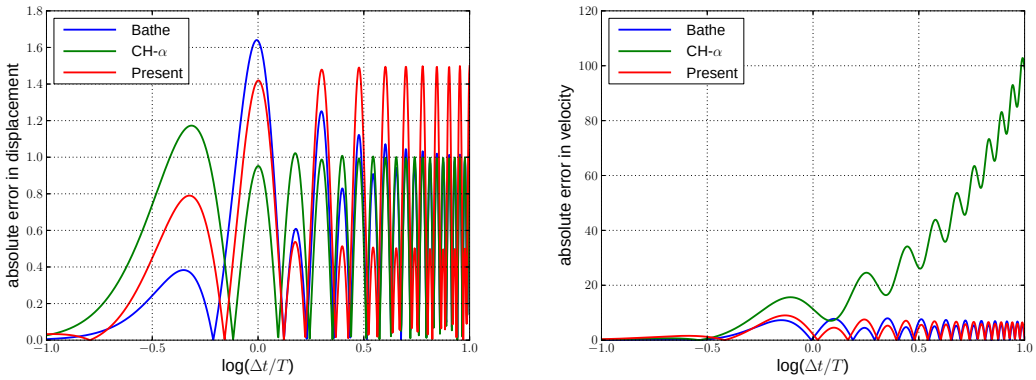

Figure 4: Overshoot analysis: absolute errors at first time step for $\xi = 0.0$ and $\rho_\infty = 0.0$.

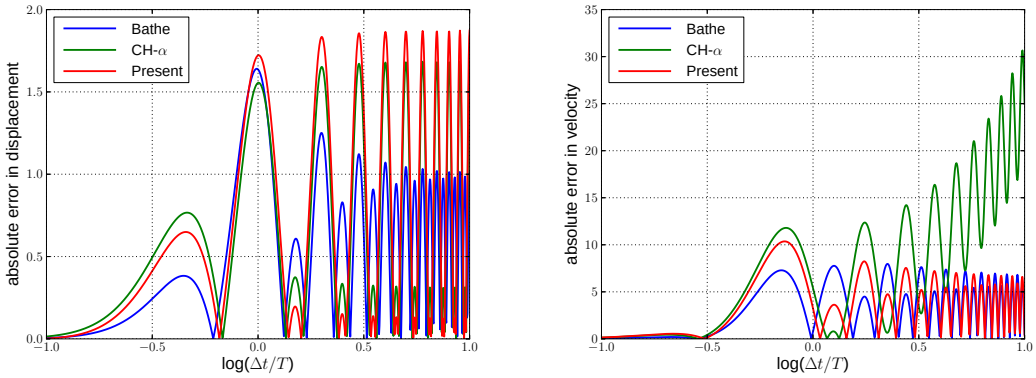

Figure 5: Overshoot analysis: absolute errors at first time step for $\xi = 0.0$ and $\rho_\infty = 0.5$.

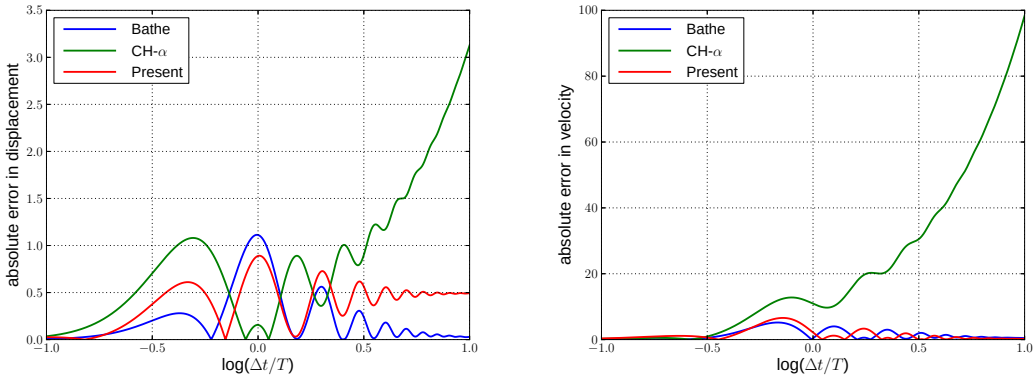

Figure 6: Overshoot analysis: absolute errors at first time step for $\xi = 0.1$ and $\rho_\infty = 0.0$.

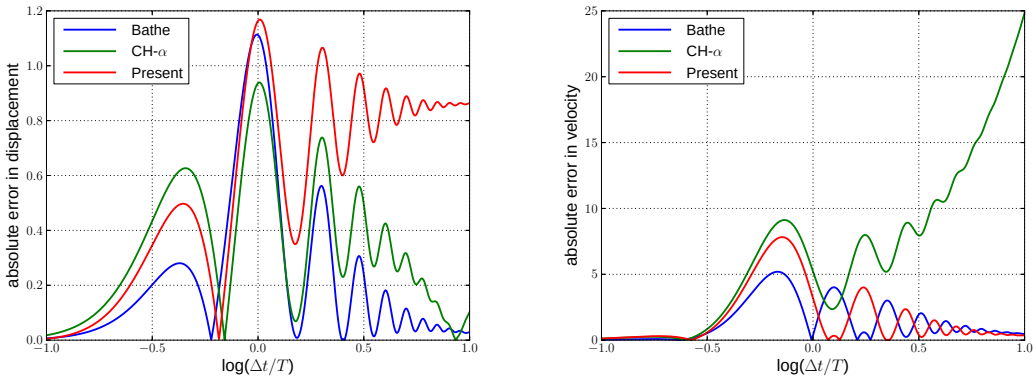

Figure 7: Overshoot analysis: absolute errors at first time step for $\xi = 0.1$ and $\rho_\infty = 0.5$.

6. Numerical examples

In this section, we apply the proposed scheme for structural dynamic problems with multiple degrees of freedom (MDOF). For this purpose, we consider a three-dof spring-mass problem, a two-dimensional Howe truss model, and an elastic pendulum modelled with non-linear truss element. Solutions obtained with the present schemes are compared with those obtained with the CH-α and Bathe's two-step schemes. As the accuracy of the computed solution(s) and the computational cost incurred are the two most important criteria when solving large-scale problems discretised with finite elements, we investigate the accuracy of the solutions obtained for the same computational cost. Here, the computational cost refers to the cost of *linear equations solver* only, ignoring level-1 and level-2 BLAS operations. Since the computational cost of Bathe's scheme, for a given time step, is twice that of CH-α and the present schemes, time step used for Bathe's scheme is chosen to be twice that of CH-α and present schemes.

6.1. Three DOF stiff-flexible spring problem

This example, adopted from Bathe and Noh [34], is shown in Fig. 8. The values of stiffness and mass are: $k_1 = 10^7$, $k_2 = 1$, $m_1 = 0$ and $m_2 = m_3 = 1$. Prescribed displacement at mass 1 is $d_1 = \sin 1.2\,t$. With two springs whose stiffnesses differ by several orders of magnitude, this example represents a simplified model of complex structural dynamical systems. The left spring with very high stiffness can either represent a rigid link or be viewed as a physical representation of penalty scheme for imposing constraint/boundary conditions. Due to the presence of high-frequency components in the solution, this problem serves as a good example to assess the *numerical damping* characteristic of a time integration technique.

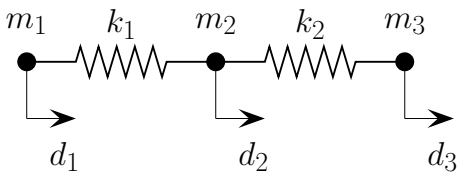

Figure 8: 3-dof example by Bathe and Noh [34].

The effective system of equations for this problem, in matrix form, is given as,

$$\begin{bmatrix} m_2 & 0 \\ 0 & m_3 \end{bmatrix} \begin{Bmatrix} \ddot{d}_2 \\ \ddot{d}_3 \end{Bmatrix} + \begin{bmatrix} k_1 + k_2 & -k_2 \\ -k_2 & k_2 \end{bmatrix} \begin{Bmatrix} d_2 \\ d_3 \end{Bmatrix} = \begin{Bmatrix} k_1\, d_1 \\ 0 \end{Bmatrix} \tag{33}$$

The initial displacement and velocity of masses 2 and 3 are zero. A time step of $\Delta t = 0.2618$ is considered. The reference solution is computed using the mode superposition technique [35]. Solutions obtained with $\rho_\infty = 0.5$ and $\rho_\infty = 0.0$ are presented in Fig. 9 and Fig. 10, respectively. For $\rho_\infty = 0.5$, the solution obtained with present scheme matches well the solution obtained with CH-α scheme and is better than the one obtained with Bathe's scheme. The difference is more pronounced in the acceleration of the node 2; and for $\rho_\infty = 0.0$, the response of node 2 obtained with the present scheme is better than that of CH-α and Bathe's scheme. While the response of node 3, obtained with $\rho_\infty = 0.0$, is poor when compared with Bathe's scheme, it is still better than the one obtained with CH-α scheme. These observations are in-line with those made for the SDOF model problem.

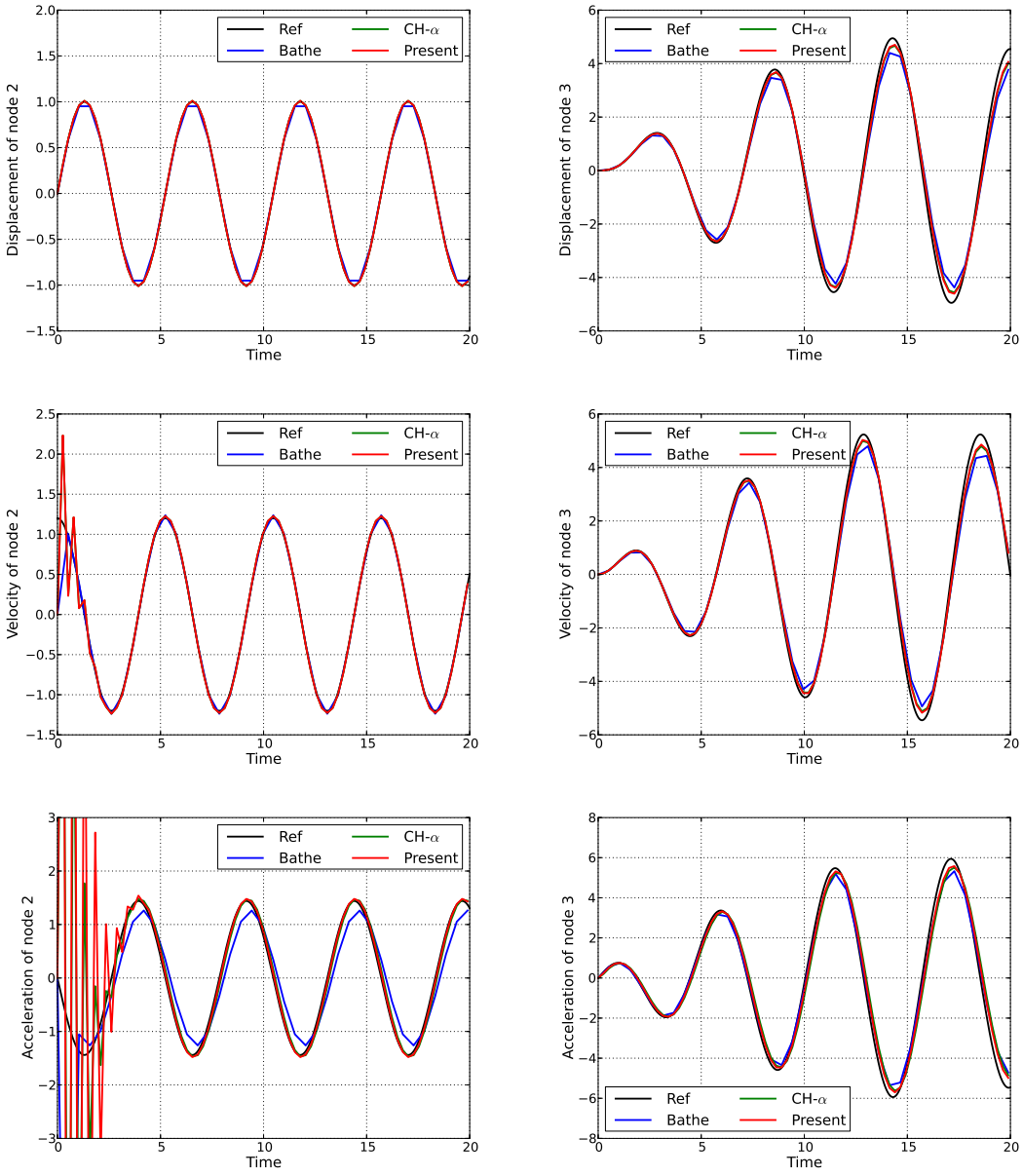

Figure 9: 3-dof example: solution obtained with $\rho_\infty = 0.5$ for CH-α and present schemes.

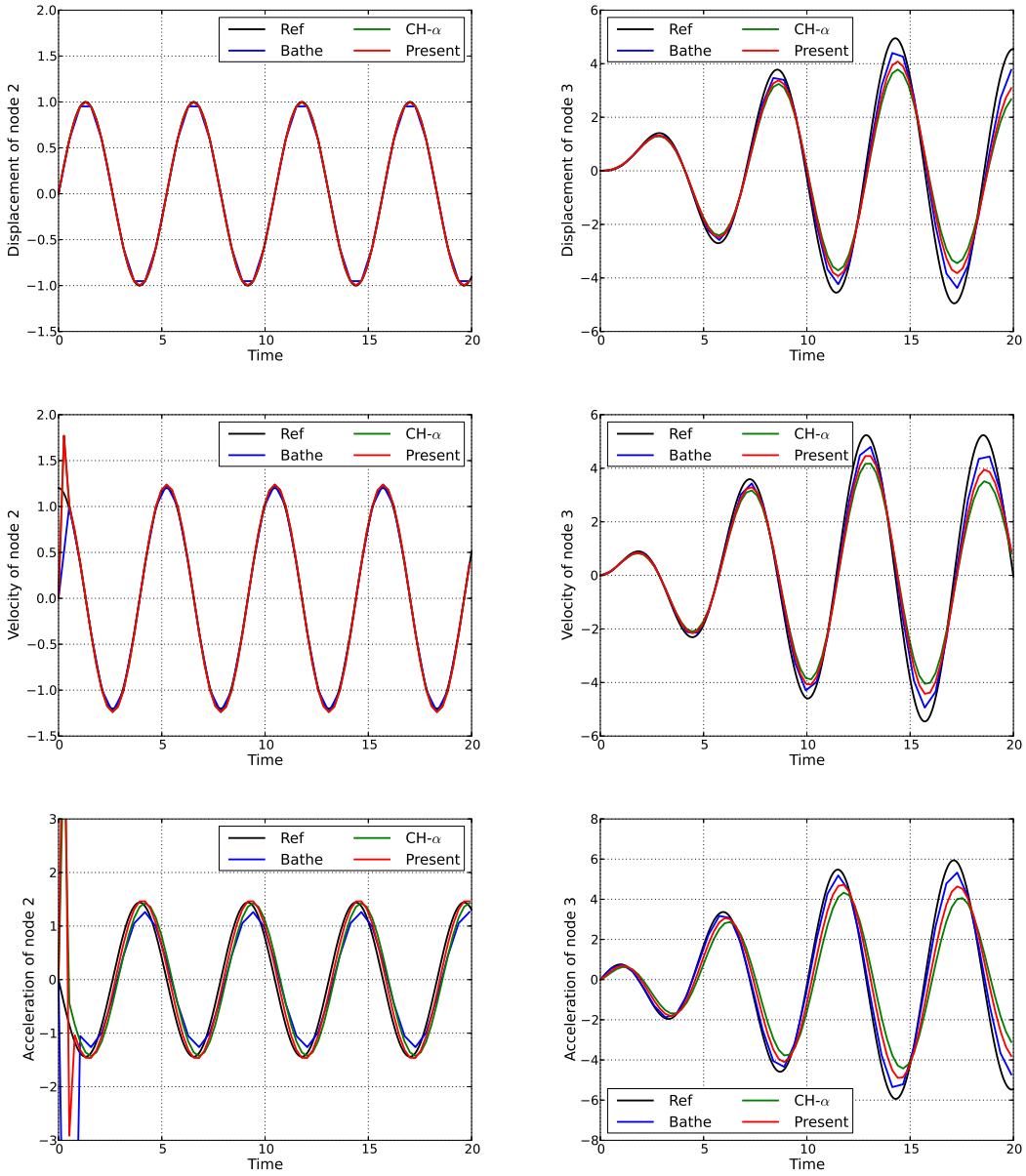

Figure 10: 3-dof example: solution obtained with $\rho_\infty = 0.0$ for CH-α and present schemes.

6.2. Howe truss model in 2D

This example is adopted from Rostami et al. [36]. Geometry and boundary conditions of the problem are as shown in Fig. 11. All the truss elements are assumed to be of uniform cross-section along their length. Area (A), density (ρ) and Young's modulus (E) considered for the analysis are: $A = 5$ in^2, $\rho = 0.289$ lb/in^3 and $E = 3 \times 10^7$ lb/in^2. The reference solution is obtained with Bathe's scheme using a time step of $\Delta t = 0.001$. A spectral radius of $\rho_\infty = 0.5$ is chosen for CH-α and present schemes. The short-term response of Y-displacement of node 8 obtained

with $\Delta t = 0.02$, and presented in Fig. 12, shows that the solution obtained with the present scheme match well with ones obtained with other two schemes as well as the reference solution. However, the long-term response, shown in Fig. 13, illustrates that the solution obtained with the present scheme is closer to the reference solution than those obtained with CH-α and Bathe's schemes. This is a direct consequence of the fact that the period error of the proposed scheme, for the same computational cost, is smaller than that of the other two schemes, as demonstrated already in Section 4.

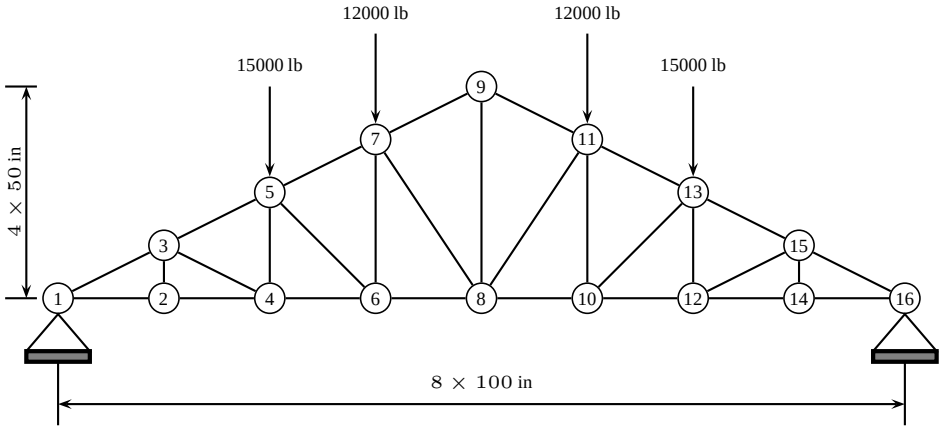

Figure 11: Howe truss model in 2D: geometry and boundary conditions.

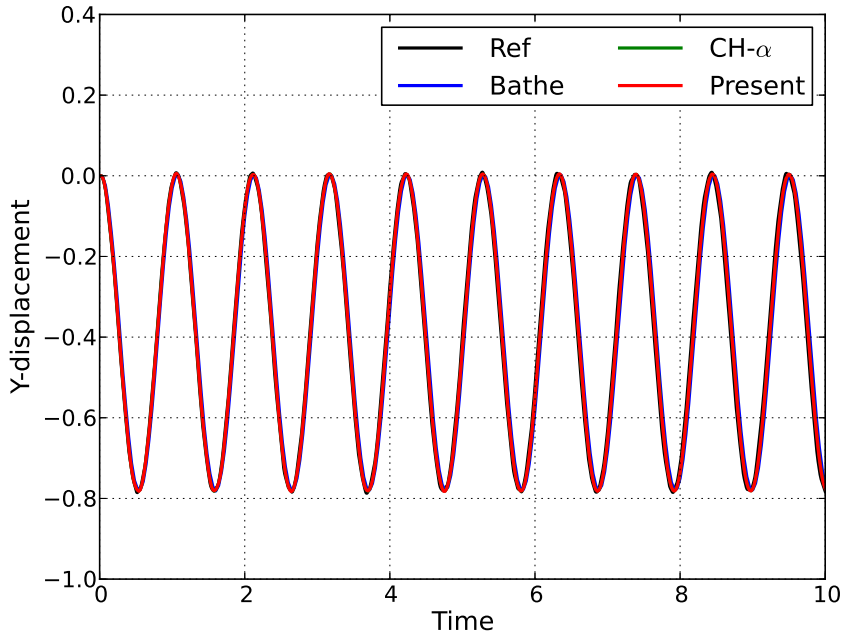

Figure 12: Howe truss model: short-term response obtained with $\Delta t = 0.02$.

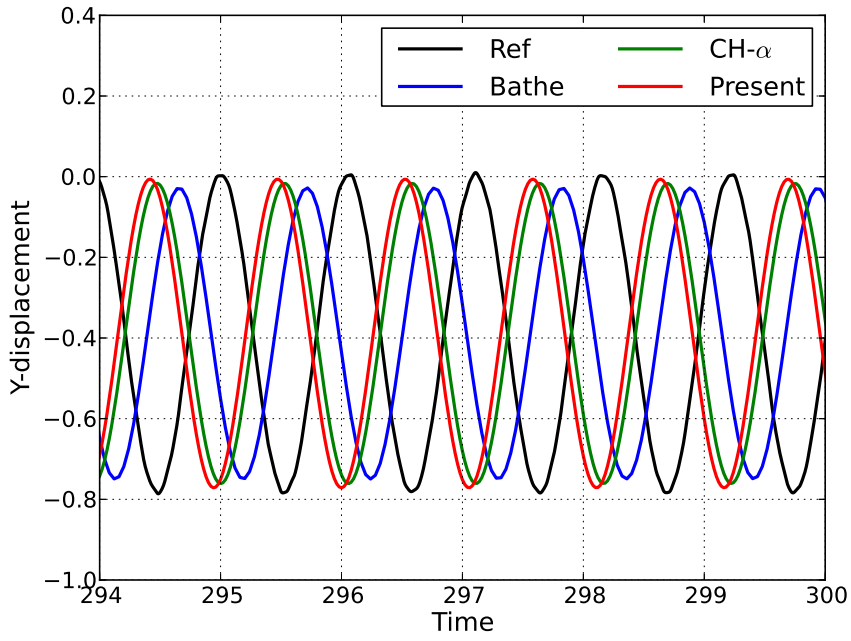

Figure 13: Howe truss model: long-term response obtained with $\Delta t = 0.02$.

6.3. Elastic pendulum

As the last example, we consider the pendulum example presented in Kuhl and Crisfield [17]. The problem consists of a pendulum with stretchable cord and is modelled with a single non-linear truss element, as shown in Fig. 14. All physical dimensions and material parameters are same as those used in [17]. The initial length is $l_0 = 3.0443$ m and mass per unit length is, $\rho_0 A_0 = 6.57$ kg/m. In this example, we consider the elastic version of the pendulum. For this case, $EA_0 = 10^4$ N, and the initial velocity and acceleration of the free node are $\dot{d}_0 = 7.72$ m/s and $\ddot{d}_0 = 0$ m^2/s, respectively.

The spectral radius for CH-α and present schemes is selected as $\rho_\infty = 0.5$. The solution obtained with $\Delta t = 0.0002$ with Bathe's scheme is used as the reference solution. Fig. 15 shows the solution obtained with $\Delta t = 0.2$. These graphs illustrate the same trend as the one observed with the single-dof model problem and previous two MDOF examples, indicating that the solution obtained with the present scheme provides better solution results than those obtained with CH-α and Bathe's schemes for the same computational cost. In order to investigate the behaviour of the solution further, simulations are carried out with a smaller time step of $\Delta t = 0.01$ and the solution is presented in Figs. 16 and 17. The short-term responses of displacement and velocity obtained with the present scheme match well with those of CH-α and Bathe's schemes, and the acceleration obtained with the present scheme is the best of all the three schemes considered. Moreover, the long-term response presented in Fig. 17 shows that, for the same computational effort, the solution obtained with the present scheme is better than those obtained with other two schemes.

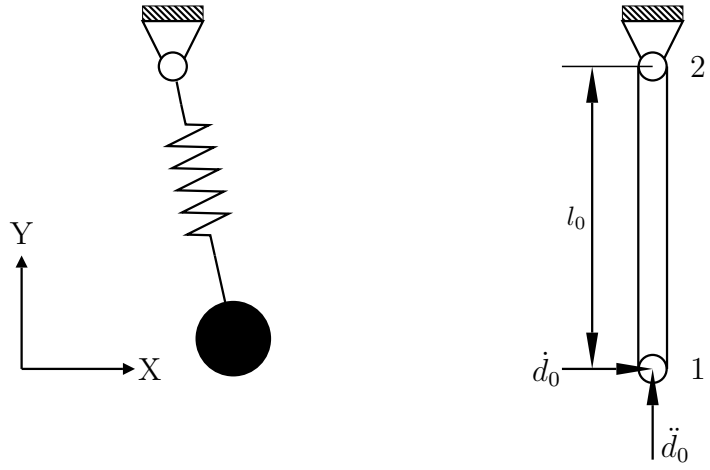

(a) Physical model (b) Truss model

Figure 14: Pendulum: problem description, boundary and initial conditions.

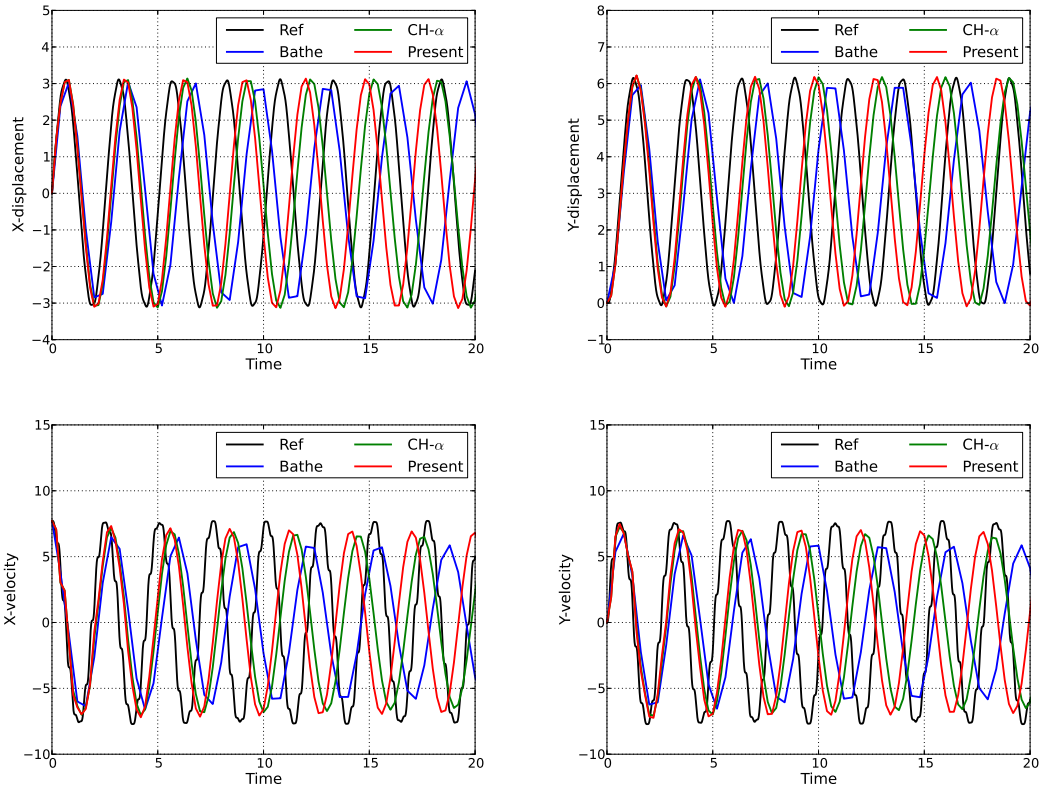

Figure 15: Elastic pendulum: solution obtained with $\Delta t = 0.2$.

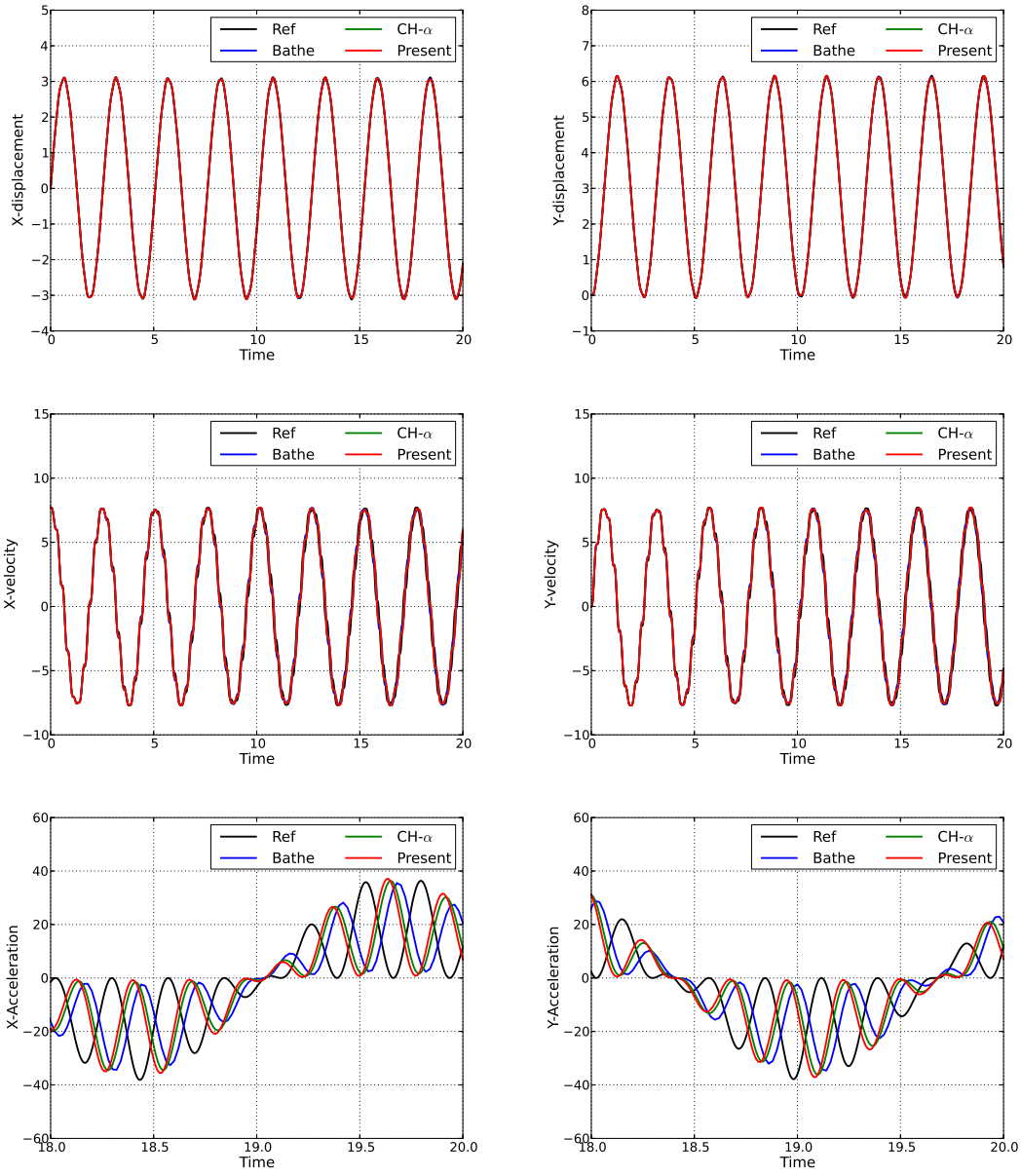

Figure 16: Elastic pendulum: short-term response obtained with $\Delta t = 0.01$.

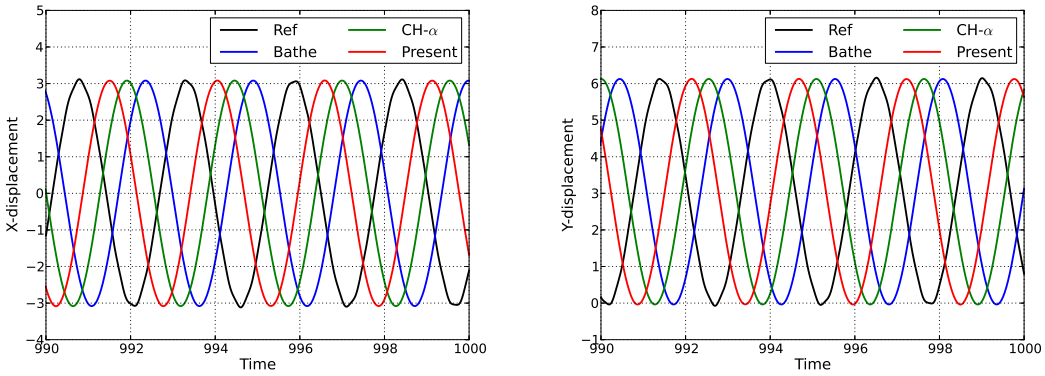

Figure 17: Elastic pendulum: long-term response obtained for the same parameters used in Fig. 16.

7. Concluding remarks

In this paper, the advantages of using the generalised-α scheme for the first-order systems, JWH-α scheme [21], for computing numerical solutions of second-order IVPs encountered in structural dynamics is presented. The governing equations are rewritten so that the proposed scheme can be easily implemented in the existing structural dynamics codes without having to convert the whole formulation into state-space. The scheme is single-step, implicit, unconditionally stable and second-order accurate. It is shown by means of spectral analysis and by studying numerical examples that the proposed scheme has improved *numerical dissipation* and *dispersion* properties when compared with the CH-α scheme. It is also demonstrated, with the SDOF model problem, that the proposed scheme does not suffer from *overshoot*.

The proposed scheme is applied to study three MDOF examples usually encountered in structural dynamics: stiff-flexible spring, Howe truss model discretised with linear truss finite elements and elastic pendulum discretised with non-linear truss elements. With these practical examples, it is illustrated that, for the same computational cost and when an appropriate value of ρ_∞ is used, the proposed scheme yields improved results, both in the case of short-term and long-term responses, when compared with CH-α and Bathe's schemes.

References

[1] J. C. Butcher. *Numerical Methods for Ordinary Differential Equations*. John Wiley & Sons Ltd, second edition, 2008.

[2] R. V. Dukkipati. *Vibration Analysis*. Alpha Science International, 2004.

[3] C. W. Gear. *Numerical Initial Value Problems in Ordinary Differential Equations*. Prentice Hall, Englewood Cliffs, NJ, 1971.

[4] D. F. Griffiths and D. J. Higham. *Numerical Methods for Ordinary Differential Equations: Initial Value Problems*. Springer, London, 2010.

[5] E. Hairer, S. P. Nørsett, and G. Wanner. *Solving Ordinary Differential Equations I: Nonstiff Problems*. Springer, Berlin, 1993.

[6] E. Hairer and G. Wanner. *Solving Ordinary Differential Equations II: Stiff and Differential-Algebraic Problems*. Springer, 1996.

[7] T. J. R. Hughes. *The Finite Element Method: Linear Static and Dynamic Finite Element Analysis*. Dover Publications, 2000.

[8] H. M. Hilber and T. J. R. Hughes. Collocation dissipation and overshoot for time integration schemes in structural dynamics. *Earthquake Engineering and Structural Dynamics*, 6:99–118, 1978.

[9] N. M. Newmark. A method of computation for structural dynamics. *Journal of the Engineering Mechanics Division (ASCE)*, 85:67–94, 1959.

[10] E. L. Wilson. A computer program for the dynamic stress analysis of underground structures. Technical report, SESM Report No. 68-1, Division of Structural Engineering and Structural Mechanics, University of California, Berkeley, CA., 1968.

[11] H. M. Hilber, T. J. R. Hughes, and R. L. Taylor. Improved numerical dissipation for time integration algorithms in structural dynamics. *Earthquake Engineering and Structural Dynamics*, 5:283–292, 1977.

[12] W. L. Wood, M. Bossak, and O. C. Zienkiwicz. An alpha modification of Newmark's method. *International Journal for Numerical Methods in Engineering*, 15:1562–1566, 1981.

[13] C. Hoff and P. J. Pahl. Development of an implicit method with numerical dissipation from generalized single-step algorithm for structural dynamics. *Computer Methods in Applied Mechanics and Engineering*, 67:367–385, 1988.

[14] J. Chung and G. M. Hulbert. A time integration algorithm for structural dynamics with improved numerical dissipation: the generalized-α method. *Journal of Applied Mechanics (ASME)*, 60:371–375, 1993.

[15] Y. KaiPing. A new family of generalized-α time integration algorithms without overshoot for structural dynamics. *Earthquake Engineering and Structural Dynamics*, 37:1389–1409, 2008.

[16] S. Erlicher, L. Bonaventura, and O. S. Bursi. The analysis of the generalized-α method for non-linear dynamic problems. *Computational Mechanics*, 28:83–104, 2002.

[17] D. Kuhl and M. A. Crisfield. Energy-conserving and decaying algorithms in non-linear structural dynamics. *International Journal for Numerical Methods in Engineering*, 45:569–599, 1999.

[18] K. J. Bathe and M. M. I. Baig. On a composite implicit time integration procedure for nonlinear dynamics. *Computers and Structures*, 83:2513–2524, 2005.

[19] W. B. Wen, K. Wei, H. S. Lei, S. Y. Duan, and D. N. Fang. A novel sub-step composite implicit time integration scheme for structural dynamics. *Computers and Structures*, 182:176–186, 2017.

[20] J. Zhang, Y. Liu, and D. Liu. Accuracy of a composite implicit time integration scheme for structural dynamics. *International Journal for Numerical Methods in Engineering*, 109:368–406, 2017.

[21] K. E. Jansen, C. H. Whiting, and G. M. Hulbert. A generalized-α method for integrating filtered Navier-Stokes equations with a stabilized finite element method. *Computer Methods in Applied Mechanics and Engineering*, 190:305–319, 2000.

[22] S. Rossi, N. Abboud, and G. Scovazzi. Implicit finite incompressible elastodynamics with linear finite elements: A stabilized method in rate form. *Computer Methods in Applied Mechanics and Engineering*, 311:208–249, 2016.

[23] X. Zeng, G. Scovazzi, N. Abboud, O. Colomés Gene, and S. Rossi. A dynamic variational multiscale method for viscoelasticity using linear tetrahedral elements. *International Journal for Numerical Methods in Engineering*, xxx:xxx–xxx, 2017.

[24] W. G. Dettmer and D. Perić. An analysis of the time integration algorithms for the finite element solutions of incompressible Navier-Stokes equations based on a stabilised formulation. *Computer Methods in Applied Mechanics and Engineering*, 192:1177–1226, 2003.

[25] W. G. Dettmer and D. Perić. A computational framework for fluid-structure interaction: Finite element formulation and applications. *Computer Methods in Applied Mechanics and Engineering*, 195:5754–5779, 2006.

[26] W. G. Dettmer and D. Perić. A computational framework for fluid-rigid body interaction: Finite element formulation and applications. *Computer Methods in Applied Mechanics and Engineering*, 195:1633–1666, 2006.

[27] W. G. Dettmer and D. Perić. A fully implicit computational strategy for strongly coupled fluid-solid interaction. *Archives of Computational Methods in Engineering*, 14:205–247, 2007.

[28] C. Kadapa, W. G. Dettmer, and D. Perić. A fictitious domain/distributed Lagrange multiplier based fluid-structure interaction scheme with hierarchical B-Spline grids. *Computer Methods in Applied Mechanics and Engineering*, 301:1–27, 2016.

[29] C. Kadapa, W. G. Dettmer, and D. Perić. A stabilised immersed boundary method on hierarchical b-spline grids for fluid-rigid body interaction with solid-solid contact. *Computer Methods in Applied Mechanics and Engineering*, 318:242–269, 2017.

[30] Y. Bazilevs, V. M. Calo, T. J. R. Hughes, and Y. Zhang. Isogeometric fluid-structure interaction: theory, algorithms, and computations. *Computational Mechanics*, 43:3–37, 2008.

[31] W. G. Dettmer and D. Perić. A new staggered scheme for fluid-structure interaction. *International Journal for Numerical Methods in Engineering*, 93:1–22, 2013.

[32] O. C. Zienkiewicz and R. L. Taylor. *The Finite Element Method for Solid and Structural Mechanics*. Elsevier Butterworth and Heinemann, Oxford, England, Sixth edition, 2005.

[33] E. A. de Souza Neto, D. Perić, and D. R. J. Owen. *Computational Methods for Plasticity, Theory and Applications*. John Wiley and Sons, United Kingdom, 2008.

[34] K. J. Bathe and G. Noh. Insight into an implicit time integration scheme for structural dynamics. *Computers and Structures*, 98-99:1–6, 2012.

[35] K. J. Bathe. *Finite Element Procedures*. Prentice Hall Inc., New Jersey, 1996.

[36] S. Rostami, S. Shojaee, and H. Saffari. An explicit time integration method for structural dynamics using cubic B-spline polynomial functions. *Scientia Iranica Transactions A: Civil Engineering*, 20:23–33, 2013.